Microelectronic Engineering 187–188 (2018) 144–147

Contents lists available at ScienceDirect

Microelectronic Engineering

journal homepage: www.elsevier.com/locate/mee

Research paper

# Strain coupling optimization in magnetoelectric transducers

D. Tierno [a,b,*], F. Ciubotaru [a], R. Duflou [a], M. Heyns [a,b], I.P. Radu [a], C. Adelmann [a]

[a] Imec, Kapeldreef 75, 3001 Leuven, Belgium
[b] KU Leuven, Departement Materiaalkunde (MTM), B-3001 Leuven, Belgium

ARTICLE INFO

*Article history:*
Received 13 October 2017
Accepted 9 November 2017
Available online 11 November 2017

*Keywords:*
Magnetoelectric effect
Strain
Transducers
Spin waves

ABSTRACT

The mechanical behavior of magnetoelectric transducers consisting of piezoelectric-magnetostrictive bilayers has been modeled. The effect of the aspect ratio of the transducer as well as the influence of non-active surrounding layers has been modeled, including a passivation layer surrounding the active device, a clamping layer above the active device, and an interfacial layer that might be inserted between the magnetostrictive and the piezoelectric layers. Strategies to control and maximize the strain magnitude and orientation based on material selection and device design are proposed.



## 1. Introduction

Current semiconductor-based CMOS devices may reach their physical limits in the next decade. To be able to continue Moore's law, to improve the device performance, and to further lower the power per operation, the replacement of CMOS circuits by novel circuits based on different physical effects may become necessary. In particular, logic circuits based on the interference of spin waves [1,2] are a promising alternative to CMOS technology and are highly suitable to efficiently implement majority gates [1–4], in which the state of the output is determined by the majority of the input states. In such spin wave logic gates, the information is encoded in the phase of the waves and the output is determined by the interference of multiple spin waves propagating in a common waveguide. Spin-wave computing has the potential for low-power computation since no charge motion takes place. Furthermore, it allows the functional scaling of the circuit [1] which would relax the high density of on chip-elements required in the CMOS technology. To build logic circuits based on spin-wave majority gates that are competitive with CMOS-based technology, it is necessary to develop energy efficient transducers between spin-wave and electric domains so to cointegrate the two technologies in a single system. Key requirements of such transducers are high coupling efficiency, low operational power, and high bandwidth [1–3]. Microwave antennae have typically been used to generate spin waves using electric currents [4,5] but are neither scalable nor energy efficient. By contrast, magnetoelectric transducers represent a scalable and low-power alternative [2,3] consisting of a piezoelectric-magnetostrictive (PE-MS) bilayer in which the coupling between the electric and the spin domain occurs via strain: when an electric field is applied across the piezoelectric, strain is induced and transferred to the magnetostrictive film that in turn changes its magnetic anisotropy via the inverse magnetostrictive effect. The resulting change of the effective magnetic anisotropy field can exert a torque on the magnetization and, in case of an AC excitation, generate spin waves.

Most of the research performed in this field has focused on the coupling mechanism of magnetoelectric bilayers. By contrast, little interest instead is shown for actual micro- or nanoscale devices. Materials with high piezoelectric and magnetostrictive coefficients are desirable for the PE-MS bilayer but strain transfer optimization within the bilayer in patterned transducers presents several integration challenges. To design efficient micro- and nanomechanical transducers width dimensions of few μm or less, many aspects need to be addressed such as the impact of the geometry of the patterned transducer as well as the mechanical properties of all materials in fully integrated magnetoelectric transducers.

The stress-strain relation is described but the Generalized Hooke's law:

$$\varepsilon_{xx} = \frac{\sigma_{xx}}{E} - \upsilon\frac{\sigma_{yy}}{E} - \upsilon\frac{\sigma_{zz}}{E} \tag{1}$$

$$\varepsilon_{yy} = -\upsilon\frac{\sigma_{xx}}{E} + \frac{\sigma_{yy}}{E} - \upsilon\frac{\sigma_{zz}}{E} \tag{2}$$

$$\varepsilon_{zz} = -\upsilon\frac{\sigma_{xx}}{E} - \upsilon\frac{\sigma_{yy}}{E} + \frac{\sigma_{zz}}{E} \tag{3}$$

with $E$ the Young's modulus of the material and $\upsilon$ the Poisson ratio.

* Corresponding author at: Kapeldreef 75, 3001 Leuven, Belgium.
*E-mail address:* davide.tierno@imec.be (D. Tierno).

https://doi.org/10.1016/j.mee.2017.11.008
0167-9317/

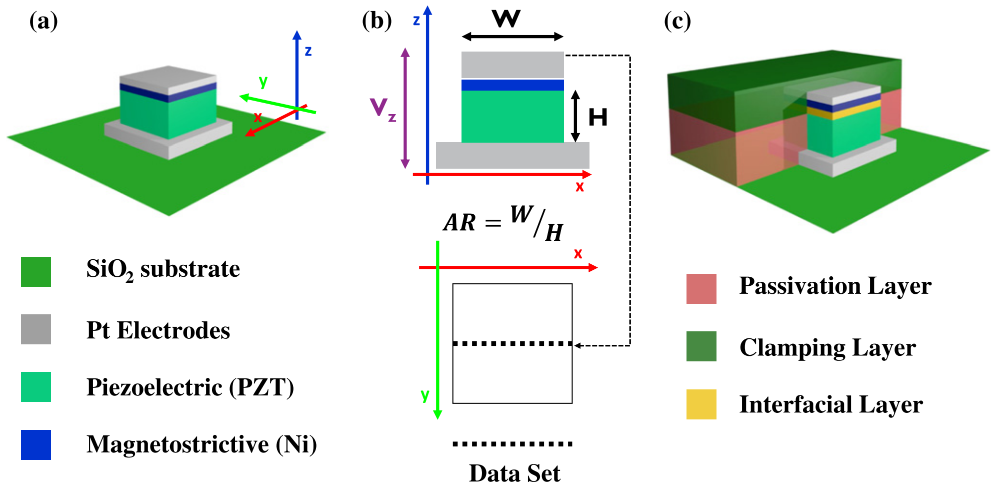


**Fig. 1.** (a) Schematic and (b) Cross-section of the rectangular cuboid magnetoelectric transducer; (c) Schematic of the magnetoelectric transducer including the non-active layers.

The magnetoelastic torque $\tau$ on the magnetization due to a strain field is given by [6]:

$$_{mel} = \begin{pmatrix} 2B_1 m_y m_z (_{yy} - _{zz}) + B_2 \left( m_z m_{xxy} - m_x m_{yzx} + \left( m_z^2 - m_y^2 \right)_{yz} \right) \\ 2B_1 m_z m_x (_{zz} - _{xx}) + B_2 \left( m_x m_{yyz} - m_y m_{zxy} + \left( m_x^2 - m_z^2 \right)_{zx} \right) \\ 2B_1 m_x m_y (_{xx} - _{yy}) + B_2 \left( m_y m_{zzx} - m_z m_{xyz} + \left( m_y^2 - m_x^2 \right)_{xy} \right) \end{pmatrix} \quad (4)$$

where $m_{x,y,z} = M_{x,y,z}/M_S$ are the normalized components of the magnetization vector $M$ with respect the saturation magnetization $M_S$, $\varepsilon_{i,j}$ are the components of the strain tensor within the magnetostrictive layer, $B_1$ and $B_2$ are the magnetoelastic coupling constants, and $\tau$ is the exerted torque, $H$ is the effective magnetic field associated with the magnetoelasticity and $\mu_0$ the permeability of vacuum.

From Eq. (4) it is obvious that $\varepsilon_{i,j}$ plays an important role on the magnitude of the torque exerted on the magnetization due to the magnetoelectric effect, and implicitly, on the excitation efficiency of spin waves. Therefore, to develop a suitable model of the transducer to define strategies and guidelines to control the magnitude and the distribution of $\varepsilon_{i,j}$ is of crucial interest. In this work, we proposed a design of a such magnetoelectric transducer and we analyzed the behavior of the strain tensor components $\varepsilon_{i,j}$ as a function of the geometrical parameters. Further, we studied the influence of additional features of the design as the presence of a passivation, interlayer or and the impact of their mechanical properties on the response of the device.

## 2. Model description

To quantitatively assess the magnetoelastic and magnetoelectric coupling in magnetoelectric transducers, the mechanical response of a rectangular cuboid transducer was studied using COMSOL Multiphysics simulations.

Of particular interest was the geometry of the transducer and the impact of the non-active surrounding layers on the effective magnetoelastic and magnetoelectric coupling. A schematic of the transducer and its cross-section are shown Fig. 1A and B, respectively. Such a geometry is perhaps the easiest to fabricate and has been proposed in several publications [7–11]. The "active" part of the structure consisted of a pillar including the magnetoelectric bilayer and two metal electrodes. Underneath, a 400 nm thick $SiO_2$ layer provided electrical insulation from the 20 μm Si substrate. The model also included an extended free area around the pillar (see Fig. 1A) so that the edges of the pillar can displace freely. This free region was set to be five times the width (W) of the pillar and scaled accordingly. The bottom face of the Si box was set as fixed in the boundary conditions of the model, which thus includes potential deformations of the substrate.

Successively, three non-active layers were added, as shown in Fig. 1C: a passivation layer surrounding the active transducers, a clamping layer above the transducer, and an interfacial layer that might be inserted between the magnetostrictive and the piezoelectric layers. The three non-active layers were added to the model one at the time to evaluate their impact individually. The range of Young's moduli used in the simulations for the three layer was defined after characterizing a set of candidate materials by nanoindentation [12,13].

Table 1 shows a more detailed summary of the geometric dimensions and the materials used in the model. Below, we quantitatively assess the variation of the magnetoelastic coupling across the different simulated scenarios with the purpose to define strategies and guidelines to optimize and engineer the strain coupling.

## 3. Results and discussion

### 3.1. Aspect ratio

We first discuss the behavior of the active transducer pillar without additional layers to evaluate the impact of the aspect ratio on the displacement of the piezoelectric layer and eventually on the coupling efficiency. Keeping the thickness H of the piezoelectric layer constant at 200 nm, the aspect ratio AR = W/H was varied between 0.1 and 100 by progressively increasing the pillar width W from 20 nm to 20 μm. The largest aspect ratios can be considered to mimic blanket layers. In all simulations below, an electric field of 50 kV/cm was applied across the magnetoelectric bilayer. The in-plane and out-of-plane

**Table 1**
Geometric dimensions and materials of the active and non-active elements of the magnetoelectric transducer.

| | Symbol/Formula | Value (or Range) | Material |
|---|---|---|---|
| Width Transducer | *W* | 20 nm–20 μm | – |
| Thickness Magnetostrictive | *tms* | 10 nm | Nickel |
| Thickness Piezoelectric | *H* | 100 nm–200 nm | PZT |
| Thickness Substrate | *tsub* | 20 um | Si |
| Thickness $SiO_2$ | *tox* | 400 nm | $SiO_2$ |
| Thickness Electrodes | *tel* | 70 nm | Pt |
| Extension Free Area | $5 \times W$ | 100 nm–100 μm | – |
| Thickness Passivation Layer | *tpass* (=*tpe*) | 100 nm–200 nm | – |
| Thickness Clamping Layer | *tclamp* | 200 nm | – |
| Thickness Interfacial Layer | *tint* | 10 nm | – |